**MAGNETIC RESONANCE**
Open Access Discussions

+ These authors have contributed equally

# Design and performance of an oversized-sample 35 GHz EPR resonator with an elevated $Q$ value

Jörg W.A. Fischer[+1], Julian Stropp[+1], René Tschaggelar[+1], Oliver Oberhänsli[1], Nicholas Alaniva[1], Mariko Inoue[2], Kazushi Mashima[2], Alexander Benjamin Barnes[1], Gunnar Jeschke[1], and Daniel Klose*[1]

[1]Institute for Molecular Physical Science, ETH Zurich, Vladimir-Prelog-Weg 2, CH-8093 Zurich, Switzerland.
[2]Department of Chemistry Graduate School of Engineering Science, Osaka University, 1–3 Machikaneyama-cho, Toyonaka, Osaka 560-8531, Japan.

**Correspondence:** *Daniel Klose (daniel.klose@phys.chem.ethz.ch)

**Abstract.**

Continuous wave EPR spectroscopy at 35 GHz is an essential cornerstone in multi-frequency EPR studies and crucial for differentiating multiple species in complex systems due to the improved g tensor resolution compared to lower microwave frequencies. Especially for unstable and highly sensitive paramagnetic centers the reliability of the measurements can be improved by the use of a single sample for EPR experiments at all frequencies. Besides the advantages, the lack of common availability of oversized-sample resonators at 35 GHz often limits scientists to lower frequencies or smaller sample geometries, the latter may be non-trivial for sensitive materials. In this work, we present the design and performance of an oversized-sample 35 GHz EPR resonator with a high loaded $Q$ value up to 3300 well suited for continuous wave EPR and single microwave frequency experiments with low excitation power. The design is driven by electromagnetic field simulations and the microwave characteristics of manufactured prototypes were found in agreement with the predictions. The resonator is based on a cylindrical cavity with a $TE_{011}$ mode allowing for 3 mm sample access. Design targets met comprise high sensitivity, robustness, ease of manufacturing and maintenance. The resonator is compatible with commercial EPR spectrometers and cryostats, allowing for measurements at temperatures down to at least 4 K. To highlight the general applicability, the resonator was tested on metal centers as well as on organic radicals featuring extremely narrow lines.

## 1 Introduction

Electron paramagnetic resonance (EPR) spectroscopy is a versatile and sensitive technique ideally suited to probe paramagnetic centers, even in complex environments such as heterogeneous catalysts. (Bonke et al., 2021) Chemical and structural information on the paramagnetic center is encoded in parameters of the effective spin Hamiltonian, describing the unpaired electron spin(s) as well as coupled magnetic nuclei. (Roessler and Salvadori, 2018; Schweiger and Jeschke, 2001) For systems with a single electron spin ($S = 1/2$) the solid-state continuous wave (CW) EPR spectra measured at the common frequency of 9.5 GHz (aka X band) are dominated by the anisotropic Zeemann interaction and the anisotropic hyperfine interaction described by the g tensor and A tensor, respectively. For the case of significant g and A anisotropy, as found in transition metal complexes,

**MAGNETIC RESONANCE**
Open Access Discussions

spectra can be several GHz broad. Accordingly, for many applications a high sensitivity is essential. Key determining factors
for the sensitivity of an EPR spectrometer are the resonator properties, including the sample volume it allows for.

In addition to sufficient sensitivity, resolution and spectral overlap are of concern for the analysis of complex samples, such
as heterogeneous catalysts, where several paramagnetic species may be present. Already for a single anisotropic paramagnetic
species, the number of parameters in the spin Hamiltonian is regularly beyond what can be resolved in a single CW EPR
spectrum. (NejatyJahromy et al., 2021) The presence of several paramagnetic species often leads to severe spectral overlap,
which occludes access to the full information on each individual species inherent in the CW EPR line shape. To alleviate
this challenge, multi-frequency EPR is employed as an essential tool to deconvolute overlapping spectral components and to
constrain the full set of the anisotropic interactions in the spin Hamiltonian. (Misra, 2011) Multi-frequency EPR typically
makes use of a combination of frequencies and corresponding magnetic field ranges with the most accessible frequencies
being ~4 GHz (S band), ~9.5 GHz (X band), ~35 GHz (Q band), and ~95 GHz (W band). This serves, first, to disentangle the
field-dependent Zeeman interaction and the field-independent hyperfine interaction, and second, to increase spectral resolution
for the g tensor at higher fields. This approach is known to aid the differentiation of multiple spectral species. For samples
with (residual) motion of the paramagnetic centers, the different frequencies are sensitive to different motional averaging time
windows. Hence, multi-frequency EPR can also enhance studies of the inherent dynamics. (Zhang et al., 2010)

For samples of limited stability, such as catalysts that are highly sensitive to oxygen or moisture, or samples that are chal-
lenging to reproduce quantitatively, such as *ex situ* freeze-trapped reaction intermediates, it is highly advantageous to record
multi-frequency EPR data on the very same sample. This requires resonators that allow for the same sample tube diameter at
different microwave frequencies. (Tschaggelar et al., 2009) This is particularly important for a quantitative global analysis by
spectral simulations (Stoll and Schweiger, 2006), where variations in relative contributions of different species between the
spectra taken at different frequencies cannot be tolerated. With sample dimensions in EPR spectroscopy being comparable to
the wavelength at least at the higher frequencies, the requirement to measure the same sample at different frequencies poses a
technical challenge. Sensitivity optimization requires larger sample volumes at lower frequencies (Misra, 2011), with sample
tube outer diameter (o.d.) of 5 mm in S band and of 4 mm in X band being typical. However, even an o.d. of 3 mm already
exceeds a quarter of the wavelength in Q band and corresponds to approximately the wavelength in W band. When we consider
a 3 mm o.d. sample tube as a reasonable compromise, the sample is thus *oversized* in these two bands. Therefore, the properties
of the resonant cavity are strongly influenced by the dielectric properties of the sample tube and sample. This poses a challenge
to the design of a robust cavity resonator, particularly for CW EPR, where adequate sensitivity requires a high quality ($Q$)
factor.

For frequencies of about 33-36 GHz in Q band, different types of resonators have been designed and evaluated. Loop-gap
resonators, originally introduced by Froncisz and Hyde (Froncisz and Hyde, 1982), are well suited to concentrate the $B_1$-field
to a limited sample volume. Several designs of Q-band loop-gap resonators were published (Mett et al., 2009; Forrer et al.,
2008; Denysenkov et al., 2017) and $B_1$-fields corresponding to a Rabi frequency of 40 MHz over bandwidths > 1 GHz were
achieved (Tschaggelar et al., 2017). However, scaling to larger sample diameters strongly deteriorates performance of loop-
gap resonators. Also for high $B_1$ and large bandwidth pulse EPR applications, a cylindrical resonator operating with the $TE_{011}$

mode was computed for an oversized sample with 3 mm o.d., whereas the actual resonator used a central dielectric ring for enhancing the $B_1$ field for a smaller sample o.d. of 1.8 mm. (Raitsimring et al., 2012) For the 3 mm o.d. that we are aiming for here, cubic box resonators in $TE_{102}$ mode (Tschaggelar et al., 2009; Polyhach et al., 2012) and cylindrical cavity resonators in $TE_{011}$ mode (Reijerse et al., 2012; Judd et al., 2022; Savitsky et al., 2013; Gromov et al., 2006; Sienkiewicz et al., 1996) have been developed for different applications. Among these, the cylindrical cavities feature a higher $Q$ factor as well as a better conversion factor, and the larger sample volumes overcompensate their poorer filling factors compared to commercial dielectric resonators. (Reijerse and Savitsky, 2017)

Here, based on the design target of a high-$Q$ Q-band resonator for oversized samples suitable for CW EPR with high sensitivity, we report on the design and performance of a robust, simple cylindrical $TE_{011}$ mode cavity resonator for 3 mm o.d. sample tubes. While suitable primarily for sensitive CW EPR experiments, the resonator can be also used for pulsed single microwave frequency experiments, particularly on spectrometers with low microwave power. The resonator design is based on electromagnetic field modeling by finite element calculations in order to minimize the effect of electric fields in the sample and optimize the $Q$ factor. The experimentally determined characteristics are in good agreement with the calculated properties, highlighting the advantage of a design approach based on electromagnetic field simulations. The resonator performance was tested on a scope of samples including a homogeneous, multi-component Ti(III)-catalyst in toluene under cryogenic conditions and at room temperature to demonstrate the general applicability. The linewidth resolution was demonstrated with an extended $N@C_{60}$ sample to be better than $10^{-2}$ mT.

## 2   Materials and methods

### 2.1   Finite element simulations of electromagnetic structures

Electric and magnetic field calculations were carried out by finite element simulations with the software CST Microwave Studio (CST GmbH, Darmstadt, Germany), which uses a volume grid discretization. The geometric structure was modeled *in silico* with all parts of the resonator in contact with the microwave fields. Out-of-resonance losses were fitted by assigning a surface conductivity of $3 \cdot 10^4$ S/m to the waveguide and other (non-ideal) surfaces. All metal structures were calculated using a surface impedance model to incorporate resistive losses. The geometry of the resonator has been parameterized and optimized in terms of center frequency, bandwidth, $B_1$ field strength, sample volume (filling height of a sample tube with 3.0 mm o.d., 2.2 mm inner diameter (i.d.)) and coupler position for different sample materials (with relative dielectric constants ranging from 1 for empty tubes up to 3 for frozen aqueous samples (Matzler and Wegmuller, 1987)). The frequency shift of the resonator upon introduction of the sample tube could be reproduced using a relative permittivity of 3.4 for the sample tube in Q band.

Simulations of the input reflection coefficient $S_{11}$ were used to describe the measured microwave reflection curves. For comparison with the experimental results obtained by a DPPH point sample, microwave field and frequency were simulated at specific locations within the resonator excluding losses and surface imperfections.

MAGNETIC
RESONANCE
Open Access
Discussions

## 2.2 Microwave reflection curve

The microwave reflection curves were measured as the scattering parameter $S_{11}$ with a calibrated network analyzer (HP 8722ES) and a source power of -10 dBm.

## 2.3 Prototype fabrication

The resonator cavity, including iris, was fabricated from a solid block of copper metal (purity 99.95%, ThyssenKrupp, Essen, Germany) by wire erosion to yield suitably smooth surfaces. The iris groove was cut from the outside by CNC milling, with the coupling rod (1 mm, copper) positioned between iris and WR28 waveguide (copper, Penn Engineering Components, Valencia, USA).

## 2.4 Sample preparation

Diphenyl-1-picrylhydrazyl (DPPH, Sigma, Buchs, Switzerland) radical powder, $N@C_{60}$ (powder, 10 ppm spin-diluted with $C_{60}$, Designer Carbon Materials Ltd., Oxford, UK) (Franco et al., 2006; Eckardt et al., 2015; Jakes et al., 2003), or standard Pittsburgh coal powder were filled into 3.0 mm o.d. (ca. 2.4 mm i.d.) samples tubes made from Heraeus HSQ300 electrically fused quartz (Aachener Quartzglas, Aachen, Germany). The titanium catalyst in toluene solution was prepared in a glovebox under Ar atmosphere by using a Ti(IV) organometallic precursor reduced to Ti(III) by triethylaluminum, details will be described elsewhere. The filling height for all samples was ca. 8 mm, except for DPPH, which was prepared using a small visible amount to approximate a point sample.

## 2.5 EPR measurements

Room temperature CW EPR measurements as well as the nutation measurements by pulse EPR were performed on a home-built pulse/CW Q band spectrometer equipped with a helium flow cryostat (CF935, Oxford Instruments, Oxfordshire) and a traveling wave tube amplifier (nominal 150 W) described by (Gromov et al., 2001). For room temperature measurements the temperature of the resonator was maintained by a gentle flow of dry nitrogen gas through the cryostat. For DPPH a microwave attenuation of 48 dB (0.32 $\mu$W), a lock-in time constant of 20.48 ms and a conversion time of 81.92 ms was used, for $N@C_{60}$ 40 dB (2 $\mu$W), 40.96 ms and 160 ms. The modulation frequency was set to 100 kHz, while the modulation amplitude was set to 0.02 mT for DPPH and to 0.002 mT for $N@C_{60}$. The Rabi nutation experiment was performed using a $t_\mathrm{p} - T - \pi/2 - \tau - \pi - \tau - echo$ pulse sequence and the input power into the resonator during the pulses was subsequently measured at the microwave bridge output with a 437B RF Power Meter (Keysight). The CW EPR spectra of the titanium catalyst were measured on a commercial EPR spectrometer (Elexsys E580, Bruker Biospin, Rheinstetten, Germany) equipped with the same helium flow cryostat as above. The Ti(III) spectra were recorded under non-saturating conditions and without overmodulation with 100 kHz modulation frequency. At room temperature 0.1 mT modulation amplitude, 161.84 ms conversion time and 36 dB microwave attenuation were used, while at 30 K the settings were 0.1 mT, 81.92 ms, and 40 dB, respectively. An overview of all measurement parameters can be found in Tab. S1.

## 3 Results and discussion

### 3.1 Resonator design

The Q-band resonator is designed for sample tubes up to 3 mm o.d. and a temperature range from 4 to 298 K in continuous He flow cryostats. Special focus was placed on low losses for a high $Q$ factor, suitability for applications with different solvents,
125    repeatable manufacturability, robust design, easy handling and cleaning. This is achieved by a cylindrical $TE_{011}$ cavity (11.5 mm diameter, 9 mm height) in a copper block and modulation coils from copper wire, which are mounted on both outer sides of the cavity block (Fig. 1a). The modulation field at the sample for a given current in the modulation coils is enhanced by horizontal slits in the copper block. With an optimized cavity height to diameter ratio, unwanted modes are suppressed or shifted out of the targeted frequency range. In case of sample damage in the cavity, the removable bottom plate of the resonator
130    allows for efficient cleaning. The microwave power is provided through a waveguide, made from copper in the bottom part and from stainless steel in the upper part to reduce thermal conductivity. The coupling of the microwave from the waveguide into the cavity is adjusted by a copper coupler in front of the iris (0.5 x 3.0 mm with rounded edges). Rotating the coupling knob at the top flange of the probehead tilts the coupler by some degrees from the vertical position and thereby changes the coupling. This is achieved by a thread just above the cavity, which converts the rotation into a tilt. The 3 mm o.d. sample tube held by
135    the tip of a sample tube holder is guided in a 8 mm vetronite tube from the top flange to the resonator at its bottom. For precise and reproducible positioning, the sample tube is inserted through a conical guide into the center of the cavity.

### 3.2 Simulations and experimental characterization of the resonator

The electromagnetic field configurations in the cavity were simulated and are depicted in Fig. 1b-e. Figure 1b and c show horizontal and vertical cross-sections through the cavity with the simulated $x$ component of the magnetic field $B_1$ of the incident
140    microwaves. Since the $x$ component of $B_1$ is orthogonal to the horizontal external magnetic field $B_0$ along $z$, the excitation of electron spins depends linearly on its strength. In Fig. 1, the space between the isolines corresponds to 6 % steps of the maximum field strength. Vertically, within $\pm 2$ mm around the position with the maximum $B_1$ field strength, the field decays to about 80 %. The horizontal, radial decay of $B_1$ inside the sample (2.2 mm inner diameter) is below 10 % and, therefore, negligible compared to the vertical decay. Spins which are located outside the vertical center region will experience a lower
145    $B_1$ field and hence will contribute to a smaller extent to the EPR signal. This is verified experimentally by the measurement of a point sample at different vertical positions in the resonator (Fig. 2). The magnetic field strength and its distribution showed only slight changes for samples with different dielectric constants.

      The electric field distribution of the $TE_{011}$ mode is shown in Fig. 1d and e. The cavity is designed such that the electric field
150    in the sample volume is minimized to avoid sample heating and a reduction of the $Q$ value due to lossy samples. (Tschaggelar et al., 2009) Samples with a high dielectric constant focus the magnetic field $B_1$ in the center. This leads to an increase in the electric field $E_1$ at the sample borders, which induces a reduction in the $Q$ value. This effect can also be seen when comparing microwave field simulations in the resonator with EPR tube (Fig. 1) and without EPR tube (Fig. **??**). Whereas for an empty
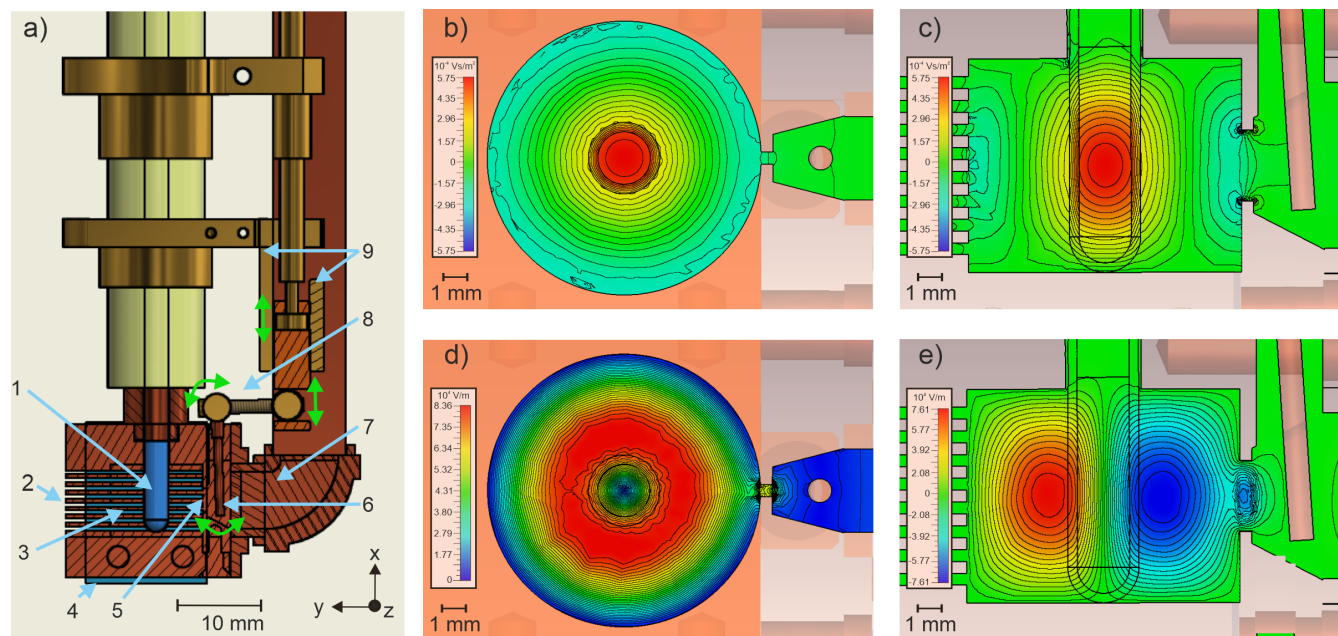
**Figure 1.** a) Rendering of the Q band EPR resonator with a cross section view of certain parts to show the technical functionality. EPR tube (1), slits for modulation field (2), cavity (3), modulation coil holder (4), iris (5), coupler (6), coupling waveguide (7), coupling mechanism (8, movement indicated by green arrows) and holder of the movable coupling piston (9); b-e) B and E field simulations with an empty quartz EPR tube ($\epsilon = 3.4$), isolines are spaced by 6 % steps of the maximum field strength with $z||B_0$; all cross sections run through the center of the cavity. b) Strength of the $x$ component of the $B_1$ field in a horizontal cross section, c) Strength of the $x$ component of the $B_1$ field in a vertical cross section, d) Strength of the tangential $E_1$ field in a horizontal cross section, e) Strength of the $z$ component of the $E_1$ field in a vertical cross section.

clear fused quartz tube the electric field penetrates only slightly into the inner part of the tube, this penetration becomes stronger
155 if the EPR tube is filled with a sample with high dielectric constant such as liquid water.

To probe the distribution of the magnetic component of the microwave field in the resonator and the shift in the resonance frequency upon sample insertion, a DPPH point sample with a defined EPR transition at g = 2.0036 was used. (Eaton et al., 2010) The inserted sample was moved in steps of 1 mm from the bottom to the upper end of the resonator cavity. The frequency of the minimum of the reflection curve was measured with an external frequency counter as a function of the sample position
160 (Fig. 2a). At each sample position, the spectrum of DPPH was measured and the double integral intensity computed (Fig. 2b). Figure 2a shows that the measured and the predicted frequency shift are in good agreement which each other for all sample positions. In Fig. 2b the normalized double integral intensity after linear baseline correction is shown in comparison with the $B_1$ field strength simulations. The measured CW EPR signal intensity of DPPH matches the one expected from simulations well. The experiment shows that the active height of the resonator is around 6 mm which corresponds to an active sample volume of
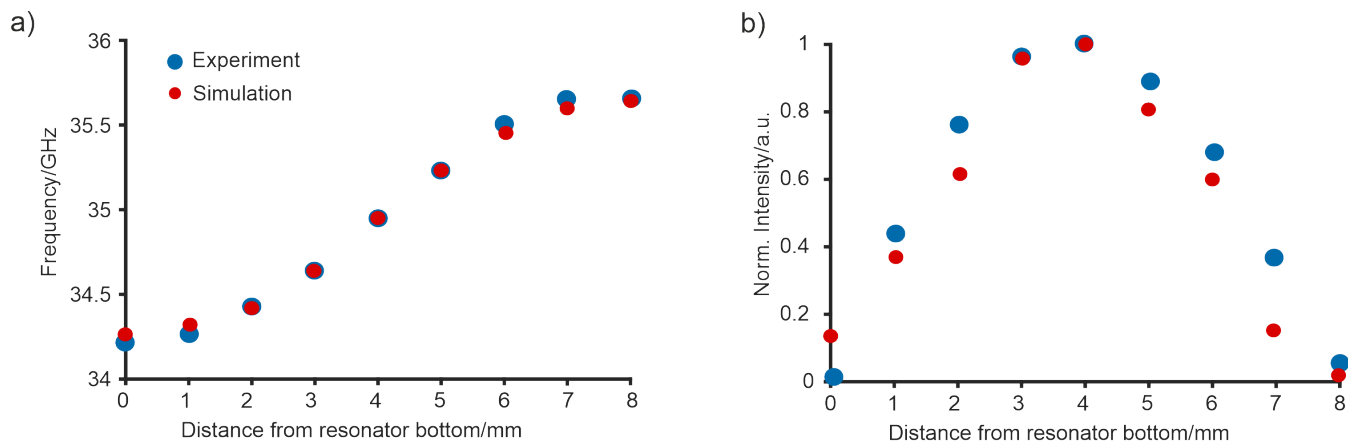
**Figure 2.** a) Frequency of the resonator mode as a function of the position of a DPPH point sample (blue) and corresponding simulations (red). b) Double integral intensity of the corresponding DPPH sample at the same positions (blue) and the expected intensity from the simulations (red).

165   about 30 µL for a 3 mm o.d. sample tube. The maximum $B_1$ field is about 3-5 mm from the bottom which corresponds to the center of the resonator.

To achieve critical coupling for a range of samples with different dielectric constants, we designed a coupling element where the angle of the copper coupling rod with respect to the iris determines the coupling strength (Fig. 1a). The design allows for a broader range to adjust the coupling compared to the previous copper ring moving vertically in front of the iris on a PEEK rod.

170   (Tschaggelar et al., 2009) Therefore, the effect of the coupler tilt angle was investigated in more detail. Figure 3 displays the simulated and experimental microwave reflection curves for different positions of the coupling element. The coupling element was moved between $-3°$ and $+3°$ around the resting position at $0°$ tilt. The frequency and $Q$ value of the resonator are in quite reasonable agreement with the simulations, although some trends slightly differ. Interestingly, the resonator features two very similar, distinct maxima in the $Q$ value at a coupling rod angle of $-3°$ and $+3°$. While in the simulations the $Q$ value

175   is higher for the $-3°$ position, in the experiment the $+3°$ position features the highest $Q$ value for an empty resonator. With an empty clear fused quartz tube, both the simulation and the experiments show that the $-3°$ features a slightly higher $Q$ value. More importantly, both experiments and simulations show a consistent increase in $Q$ value for all coupler tilt angles upon inserting the tube. This effect probably results from the tube acting as a dielectric ring that slightly pulls the electric field into the tube walls, as seen on closer inspection of Fig. 1e. This in turn leads to a reduction of the electric field near the

180   resonator walls. Additional simulations (not shown) demonstrate that the observed broadband absorption of around 4 dB in all curves can be explained by the losses introduced by the top part of the waveguide made out of stainless steel, which is used to reduce the heat flow from the flange at room temperature to the cold resonator; these losses can be strongly alleviated by silver coating of the waveguide's inner walls. (Tschaggelar et al., 2009; Himmler et al., 2022) The experimental and simulated resonator characteristics can be found in Table 1. The slight deviation between the center frequency of the simulations and the
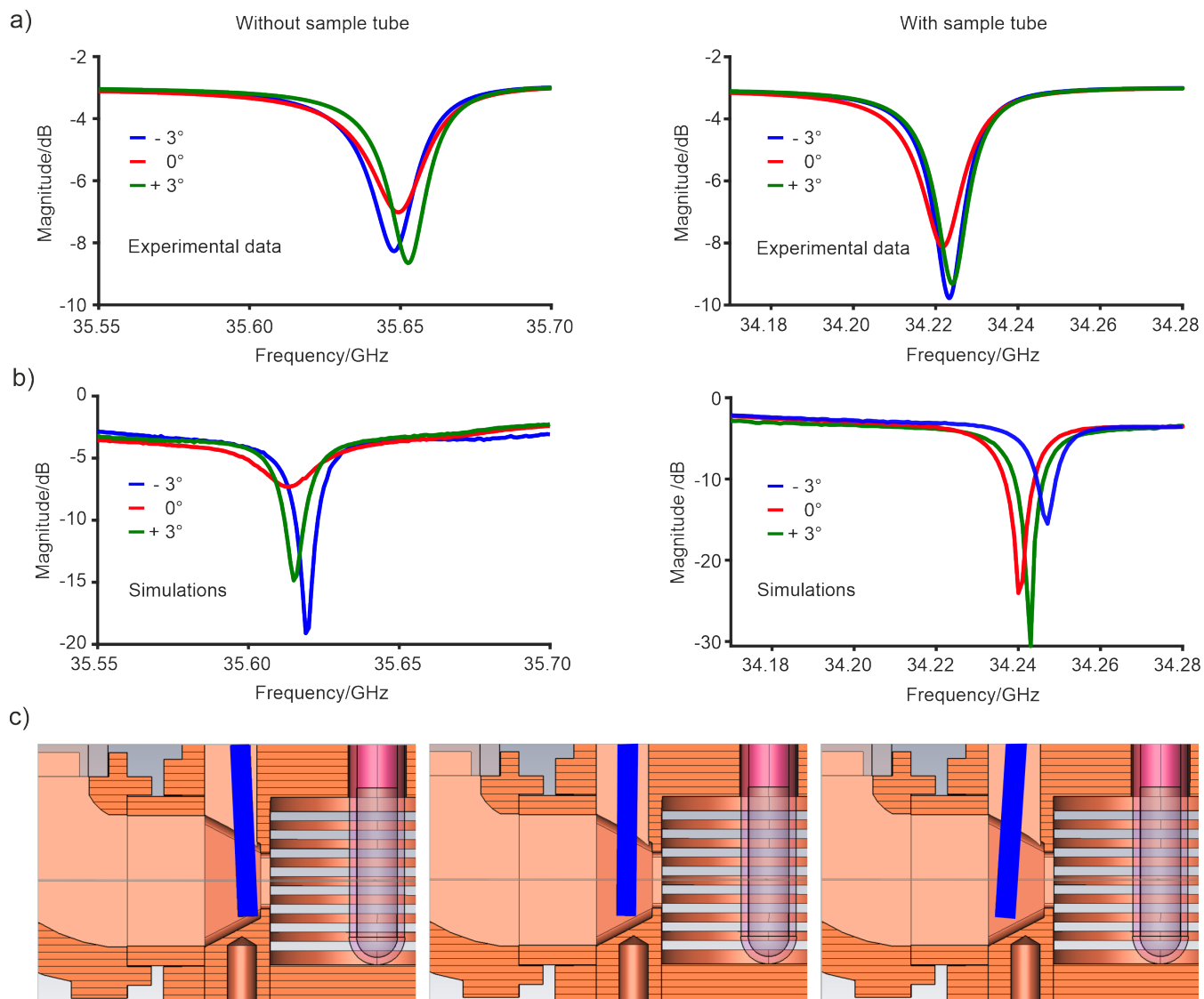
**Figure 3.** a): Experimental frequency of the resonator mode as a function of the coupler position (tilt angle) without and with a clear fused quartz sample tube. No additional modes are observed in the range of 34 - 36 GHz. b) the corresponding simulations with the same color code. c) Positions of the coupler used for the simulation from left to right $-3°$ to $+3°$. The coupling element is highlighted in blue.

experiment is most probably due to the non-perfect manufacturing of the surfaces, which leads to a decrease in the surface conductivity of the resonator material.

**Table 1.** Microwave characteristics of the resonator: Experimental and simulated resonator mode for different coupler positions (tilt angle) with and without a 3 mm o.d. clear fused quartz tube.

| | | Without tube | | | With tube | | |
|---|---|---|---|---|---|---|---|
| | Position | $f_{center}$/GHz | Bandwidth/MHz | $Q$ value | $f_{center}$/GHz | Bandwidth/MHz | $Q$ value |
| | $-3°$ | 35.62 | 14.9 | 2370 | 34.246 | 10.2 | 3350 |
| Experiment | $0°$ | 35.613 | 16.6 | 2157 | 35.613 | 14 | 2440 |
| | $+3°$ | 35.615 | 15.4 | 2290 | 34.242 | 18.2 | 2536 |
| | $-3°$ | 35.648 | 14.6 | 2441 | 34.246 | 9.4 | 3640 |
| Simulation | $0°$ | 35.656 | 13.1 | 2721 | 34.222 | 9.6 | 3565 |
| | $+3°$ | 35.652 | 13.6 | 2621 | 34.224 | 9.5 | 3602 |

### 3.3 Microwave characteristics of the resonator

In order to assess the sensitivity of the EPR resonator, we quantify contributions to the EPR signal that characterize the resonator. The intensity of a CW EPR signal in the linear regime (no saturation) can be expressed as

$$S = \chi" Q_L \eta \sqrt{PZ} \tag{1}$$

where $S$ is the signal voltage at the end of the transmission line connected to the resonator. $\chi"$ is the magnetic susceptibility of the sample, $Q_L$ is the loaded quality factor of the resonator, see Equation (2), $\eta$ is the filling factor as defined in Equation (3), $P$ is the microwave power and $Z$ is the characteristic impedance of the transmission line. (Eaton et al., 2010) Equation (1) shows that the signal-to-noise ratio can be optimized by increasing $Q_L$ or $\eta$. The loaded quality factor $Q_L$ is defined as the ratio of the resonator frequency ($\omega$) to the width of the resonance ($\Delta\omega$),

$$Q_L = \frac{\omega}{\Delta\omega} \ , \tag{2}$$

including ohmic losses and is measured at the end of the waveguide connecting the cavity to the microwave bridge. The $Q_L$ value is a measure for the efficiency of the cavity to store microwave energy rather than dissipating it. Accordingly, it can also be defined as the ratio between the energy stored in the resonator and the energy lost per cycle. The obtained $Q_L$ value of 3350 at critical coupling is on the higher end of previously reported values for home-built Q band resonators based on the $TE_{011}$ mode (see Table 2), similar values were obtained by resonators with oversized sample tube diameters, e.g. 2.8 mm o.d. with the $Q_L$ value of 2480 by (Judd et al., 2022) and 3.0 mm o.d. with the $Q_L$ value of 2600 by (Reijerse et al., 2012).

Although the introduction of an oversized lossy sample is expected to cause a reduction in the $Q$ value, the overall sensitivity can still be higher due to the larger sample volume, which implies a larger number of spins at given concentration. (Tschaggelar et al., 2009) The enhancement of concentration sensitivity by an increase in sample volume profits from a high filling factor $\eta$, which is the ratio of the $B_1^2$-weighted integrated volume over the sample and over the whole cavity (Eaton et al., 2010),

$$\eta = \frac{\int_{sample} B_1^2 dV}{\int_{cavity} B_1^2 dV} \ . \tag{3}$$

Simulations show for the present Q band $TE_{011}$ resonator $\eta = 0.31$ with a 6 mm high sample in a 3 mm o.d. clear fused quartz tube, which is considerably higher than for a $TE_{102}$ rectangular resonator with $\eta = 0.096$ (published previously, see Table 2).

210 This significant improvement is due to better focusing of the $B_1$ field along the axis of the sample tube in the cylindrical cavity compared to the rectangular cavity. As a side effect, the resonance frequency of this high-$\eta$ cavity is more susceptible to changes in the sample position compared to the $TE_{102}$ resonator because the sample diameter is of similar size as the microwave length and a high proportion of the microwave field interacts with the sample (Fig. 1).

Ultimately, the signal intensity is driven by the strength of the $B_1$ field. The relation between the applied power (Equation

215 (1)) and $B_1$ is defined as the conversion factor ($C$),

$$C = \frac{B_1}{\sqrt{P}} \, . \tag{4}$$

$B_1$ can be calculated from the length of a $\pi$ pulse in a Rabi nutation experiment. For a coal powder sample and a Ti(III) complex in frozen toluene solution, using low-power microwave excitation, we obtain a resulting $\pi$ pulse length of 54 ns and 46 ns (Fig. S2), corresponding to conversion factors of 0.14 mT/$\sqrt{W}$ and 0.39 mT/$\sqrt{W}$, respectively, which is similar to

220 previously published resonators (see Tab. 2).

**Table 2.** Comparison of microwave characteristics with resonators from the literature. [a]empty 3mm tube, n.d.: not determined. Ranges of $Q_L$ values span the range from overcoupled to critically coupled. [b]Range are over several overcoupled three-loop-two-gap resonators. Note that $Q_L$ and conversion factor also depend on dielectric losses in a particular sample.

| Resonator type | $Q_L$ | $\eta$ | Conversion factor in mT/$\sqrt{W}$ | Tube diameter | Reference |
|---|---|---|---|---|---|
| $TE_{011}$ | $1500 - 3350$ | 0.31 | 0.14 - 0.39 | 3mm | This work |
| $TE_{011}$ | 450 - 950 | n.d. | 0.009 | 4 mm | (Gromov et al., 2006) |
| $TE_{011}$ | $1300 - 2600$ [a] | n.d. | 0.45 | 3 mm | (Reijerse et al., 2012) |
| $TE_{102}$ | $200 - 400$ [a] | 0.096 | 0.11 | 2.9 mm | (Tschaggelar et al., 2009) |
| Loop gap[b] | 250 - 700 | n.d. | 0.39 - 1.7 | 0.4 - 1.6 mm | (Forrer et al., 2008) |

### 3.4 CW EPR performance of the resonator

To demonstrate the sensitivity and spectral resolution of the Q-band resonator on relevant systems for current research applications, we measured room temperature and low temperature (30 K) CW EPR spectra of a homogeneous Ti(III)-catalyst in toluene (Fig. 4). The Q-band CW EPR spectrum is an important complement to S-band and X-band spectra to resolve the

225 different overlapping Ti(III) species present in this system with only slightly different g tensor values. In the room-temperature Q-band CW spectrum (Fig. 4b), three major components could be readily identified. In the low-temperature spectrum, in the absence of motional averaging, the full g anisotropy of the different components is observed. Echo-detected field sweeps (by pulse EPR) are not always a full substitute for CW EPR spectra since species may have different and field-dependent relaxation times. As a result the observed relative intensities of the different species will differ between CW and pulse EPR spectra, with

230 only the CW EPR double integral intensities in the absence of saturation being insensitive to relaxation time differences. The

potential dependence of relative signal intensities on the magnetic field complicates global fitting with other frequency bands for echo-detected field-swept EPR spectra and hence hampers a quantitative analysis. In the case at hand, with the two Q-band CW EPR spectra, the g tensors of the three main components become sufficiently constrained. Together with the hyperfine couplings to surrounding nuclei, which are more clearly visible in the lower frequency spectra, we established multi-frequency

235 CW EPR analysis in S, X, and Q bands on the same sample tube as an essential step to deconvolute overlapping spectral components and to understanding the catalytic mechanism of this class of systems.

The resolution limit of the resonator was tested with spin-diluted N@$C_{60}$, which is shown in Fig. 4c. In this sample, atomic nitrogen (S = 3/2, I = 1) is trapped in the center of the fullerene $C_{60}$, which makes the g tensor and the hyperfine coupling to the nitrogen very isotropic (Almeida Murphy et al., 1996; Weidinger et al., 1998; Wittmann et al., 2018). In the room temperature

240 Q-band CW EPR spectrum recorded with a single scan, one can observe three lines due to the $^{14}$N hyperfine coupling, with each of the lines having a peak-to-peak linewidth of 0.01 mT. This establishes a resolution of at least 0.01 mT with this probehead for samples filling the whole cavity and this demonstrates sufficient homogeneity of the static magnetic field $B_0$ over a sample height of 8 mm.
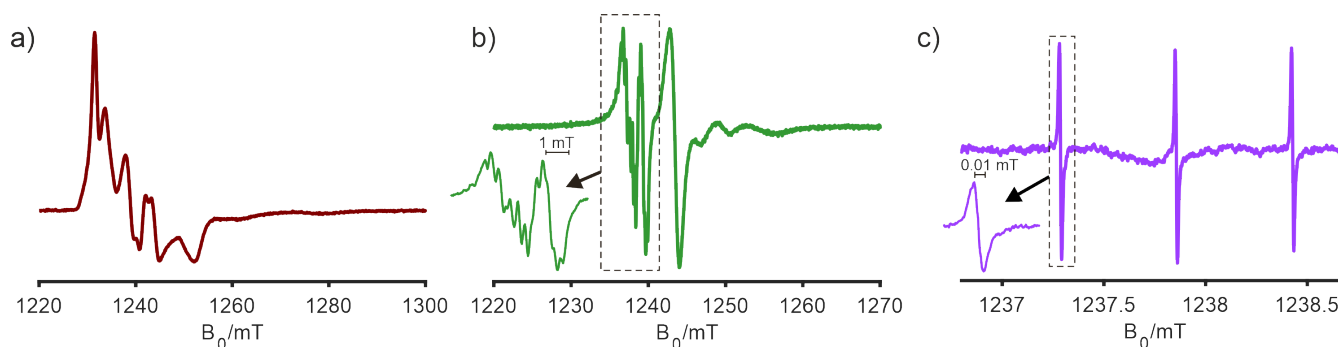


**Figure 4.** Q-band CW EPR spectra of a multi-component Ti(III)-complex system in toluene at 30 K (a), at room temperature (b), and spectrum of N@$C_{60}$ spin-diluted in $C_{60}$ at room temperature (c). The latter was measured on an extended sample (ca. 8 mm) with a modulation amplitude of 2 $\mu$T and shows an intrinsic line width of 10 $\mu$T.

## 4 Conclusion

245 In this work, we introduced the design and fabrication of a 35 GHz cavity resonator for oversized samples and evaluated its performance in CW EPR and low power pulse EPR. The cylindrical resonator employs the TE$_{011}$ mode, features a high filling factor of $\eta = 0.31$ and a high loaded $Q$ value of around 3300 when critically coupled, or an overcoupled bandwidth of about 25 MHz in combination with a 3 mm o.d. clear fused quartz tube. Electromagnetic field calculations are in good agreement with the experiments highlighting the importance of rational resonator design and simulation as a tool for geometry optimization.

250 In spite of the oversized sample geometry, a high resolution was demonstrated with a linewidth of 10 $\mu$T for N@$C_{60}$. A

Ti(III)-catalyst with multiple spectral species was employed to demonstrate general applicability of the probehead, operation at cryogenic temperatures, and the benefit for resolving spectral overlap in complex systems. This resonator is therefore very well suited for CW EPR as well as for single-frequency pulsed EPR experiments with low-power excitation. Since the construction of the resonator is straightforward due to its simplistic and robust design, we hope that it will be leveraged to enhance the use

255  of Q band in multi-frequency EPR analyses.

*Code and data availability.*  Design 3D CAD data is made available via Zenodo with DOI 10.5281/zenodo.11082486.

*Author contributions.*  DK conceived the project and data processing. JS and JF performed the experimental work and data processing. RT and DK designed the resonator, RT performed the simulations analyzed by RT and DK. OO fabricated the resonator. NA, AB, MI, and KM provided relevant test samples. JS, JF, RT and DK wrote the manuscript with input from all authors. All authors discussed the results and

260  contributed to the final manuscript.

*Competing interests.*  The authors declare that they have no conflict of interest.

**MAGNETIC**
**RESONANCE**
Open Access
Discussions

# References

265 Almeida Murphy, T., Pawlik, T., Weidinger, A., Höhne, M., Alcala, R., and Spaeth, J.-M.: Observation of Atomlike Nitrogen-Implanted Solid C60, Phys. Rev. Lett., 77, 1075–1078, https://doi.org/10.1103/PhysRevLett.77.1075, 1996.

Bonke, S. A., Risse, T., Schnegg, A., and Brückner, A.: In situ electron paramagnetic resonance spectroscopy for catalysis, Nature Reviews Methods Primers, 1, https://doi.org/10.1038/s43586-021-00031-4, 2021.

Denysenkov, V., van Os, P., and Prisner, T. F.: Q-Band Loop-Gap Resonator for EPR Applications with Broadband-Shaped Pulses, Appl.
270 Magn. Reson., 48, 1263–1272, https://doi.org/10.1007/s00723-017-0930-9, 2017.

Eaton, G. R., Eaton, S. S., Barr, D. P., and Weber, R. T.: Quantitative EPR, Springer Vienna, https://doi.org/10.1007/978-3-211-92948-3, 2010.

Eckardt, M., Wieczorek, R., and Harneit, W.: Stability of C60 and N@C60 under thermal and optical exposure, Carbon, 95, 601–607, https://doi.org/10.1016/j.carbon.2015.08.073, 2015.

275 Forrer, J., García-Rubio, I., Schuhmam, R., Tschaggelar, R., and Harmer, J.: Cryogenic Q-band (35GHz) probehead featuring large excitation microwave fields for pulse and continuous wave electron paramagnetic resonance spectroscopy: Performance and applications, J. Magn. Reson., 190, 280–291, https://doi.org/10.1016/j.jmr.2007.11.009, 2008.

Franco, L., Ceola, S., Corvaja, C., Bolzonella, S., Harneit, W., and Maggini, M.: Synthesis and magnetic properties of N@C60 derivatives, Chem. Phys. Lett., 422, 100–105, https://doi.org/10.1016/j.cplett.2006.02.046, 2006.

280 Froncisz, W. and Hyde, J. S.: The loop-gap resonator: a new microwave lumped circuit ESR sample structure, J. Magn. Reson. (1969), 47, 515–521, https://doi.org/10.1016/0022-2364(82)90221-9, 1982.

Gromov, I., Shane, J., Forrer, J., Rakhmatoullin, R., Rozentzwaig, Y., and Schweiger, A.: A Q-Band Pulse EPR/ENDOR Spectrometer and the Implementation of Advanced One- and Two-Dimensional Pulse EPR Methodology, J. Magn. Reson., 149, 196–203, https://doi.org/10.1006/jmre.2001.2298, 2001.

285 Gromov, I., Forrer, J., and Schweiger, A.: Probehead operating at 35GHz for continuous wave and pulse electron paramagnetic resonance applications, Rev. Sci. Instrum., 77, https://doi.org/10.1063/1.2216849, 2006.

Himmler, A., Albannay, M. M., von Witte, G., Kozerke, S., and Ernst, M.: Electroplated waveguides to enhance DNP and EPR spectra of silicon and diamond particles, Magn. Reson., 3, 203–209, https://doi.org/10.5194/mr-3-203-2022, 2022.

Jakes, P., Dinse, K.-P., Meyer, C., Harneit, W., and Weidinger, A.: Purification and optical spectroscopy of N@C60, Phys. Chem. Chem.
290 Phys., 5, 4080, https://doi.org/10.1039/b308284a, 2003.

Judd, M., Jolley, G., Suter, D., Cox, N., and Savitsky, A.: Dielectric Coupler for General Purpose Q-Band EPR Cavity, Appl. Magn. Reson., 53, 963–977, https://doi.org/10.1007/s00723-021-01404-4, 2022.

Matzler, C. and Wegmuller, U.: Dielectric properties of freshwater ice at microwave frequencies, J. Phys. D Appl. Phys., 20, 1623, https://doi.org/10.1088/0022-3727/20/12/013, 1987.

295 Mett, R. R., Sidabras, J. W., and Hyde, J. S.: Coupling of waveguide and resonator by inductive and capacitive irises for EPR spectroscopy, Appl. Magn. Reson., 35, 285–318, https://doi.org/10.1007/s00723-008-0162-0, 2009.

Misra, M.: Multifrequency Electron Paramagnetic Resonance: Theory and Applications, Wiley, https://doi.org/10.1002/9783527633531, 2011.

NejatyJahromy, Y., Roy, S. C., Glaum, R., and Schiemann, O.: Multi-Frequency and Single-Crystal EPR on V4+ in W-Doped $\beta$-Vanadyl(V)
300    Phosphate: Hyperfine Coupling- and g-Tensor Values and Orientation, Appl. Magn. Reson., 52, 169–175, https://doi.org/10.1007/s00723-020-01303-0, 2021.

Polyhach, Y., Bordignon, E., Tschaggelar, R., Gandra, S., Godt, A., and Jeschke, G.: High sensitivity and versatility of the DEER experiment on nitroxide radical pairs at Q-band frequencies, Phys. Chem. Chem. Phys., 14, 10 762, https://doi.org/10.1039/c2cp41520h, 2012.

Raitsimring, A., Astashkin, A., Enemark, J. H., Blank, A., Twig, Y., Song, Y., and Meade, T. J.: Dielectric Resonator for K a-Band
305    Pulsed EPR Measurements at Cryogenic Temperatures: Probehead Construction and Applications, Appl. Magn. Reson., 42, 441–452, https://doi.org/10.1007/s00723-012-0313-1, 2012.

Reijerse, E. and Savitsky, A.: Electron Paramagnetic Resonance Instrumentation, https://doi.org/10.1002/9780470034590.emrstm1511, 2017.

Reijerse, E., Lendzian, F., Isaacson, R., and Lubitz, W.: A tunable general purpose Q-band resonator for CW and pulse EPR/ENDOR
310    experiments with large sample access and optical excitation, J. Magn. Reson., 214, 237–243, https://doi.org/10.1016/j.jmr.2011.11.011, 2012.

Roessler, M. M. and Salvadori, E.: Principles and applications of EPR spectroscopy in the chemical sciences, Chem. Soc. Rev., 47, 2534–2553, https://doi.org/10.1039/c6cs00565a, 2018.

Savitsky, A., Grishin, Y., Rakhmatullin, R., Reijerse, E., and Lubitz, W.: An improved coupling design for high-frequency TE011 electron
315    paramagnetic resonance cavities, Rev. Sci. Instrum., 84, https://doi.org/10.1063/1.4788735, 2013.

Schweiger, A. and Jeschke, G.: Principles of Pulse Electron Paramagnetic Resonance, Oxford University Press, https://doi.org/10.1093/oso/9780198506348.001.0001, 2001.

Sienkiewicz, A., Smith, B. G., Veselov, A., and Scholes, C. P.: Tunable Q-band resonator for low temperature electron paramagnetic resonance/electron nuclear double resonance measurements, Rev. Sci. Instrum., 67, 2134–2138, https://doi.org/10.1063/1.1147027, 1996.

320    Stoll, S. and Schweiger, A.: EasySpin, a comprehensive software package for spectral simulation and analysis in EPR, J. Magn. Reson., 178, 42–55, https://doi.org/10.1016/j.jmr.2005.08.013, 2006.

Tschaggelar, R., Kasumaj, B., Santangelo, M. G., Forrer, J., Leger, P., Dube, H., Diederich, F., Harmer, J., Schuhmann, R., García-Rubio, I., and Jeschke, G.: Cryogenic 35GHz pulse ENDOR probehead accommodating large sample sizes: Performance and applications, J. Magn. Reson., 200, 81–87, https://doi.org/10.1016/j.jmr.2009.06.007, 2009.

325    Tschaggelar, R., Breitgoff, F. D., Oberhänsli, O., Qi, M., Godt, A., and Jeschke, G.: High-Bandwidth Q-Band EPR Resonators, Appl. Magn. Reson., 48, 1273–1300, https://doi.org/10.1007/s00723-017-0956-z, 2017.

Weidinger, A., Waiblinger, M., Pietzak, B., and Almeida Murphy, T.: Atomic nitrogen in C60:N@C60, Appl. Phys. A-Mater., 66, 287–292, https://doi.org/10.1007/s003390050668, 1998.

Wittmann, J., Can, T., Eckardt, M., Harneit, W., Griffin, R., and Corzilius, B.: High-precision measurement of the electron spin g factor
330    of trapped atomic nitrogen in the endohedral fullerene N@C60, J. Magn. Reson., 290, 12–17, https://doi.org/10.1016/j.jmr.2018.02.019, 2018.

Zhang, Z., Fleissner, M. R., Tipikin, D. S., Liang, Z., Moscicki, J. K., Earle, K. A., Hubbell, W. L., and Freed, J. H.: Multi-frequency Electron Spin Resonance Study of the Dynamics of Spin Labeled T4 Lysozyme, J. Phys. Chem. B, 114, 5503–5521, https://doi.org/10.1021/jp910606h, 2010.